Chapter 5

Wide field of view common path lateral shearing Digital Holographic Interference Microscope

5.1   Introduction

Considering the advantage of separating out different diffracted beams in frequency spectrum in off axis geometry [2, 69, 70], two beam setups are usually used for DHIM [3, 4, 5, 20, 22, 25, 26, 27, 31, 34, 36, 41, 45, 72, 73, 74, 75, 76, 77, 78, 79, 80, 105, 108, 109]. Chapter 3 and Chapter 4 discussed the use of two-beam off-axis Digital Holographic Microscope employing Mach-Zehnder geometry and its application in quantitative imaging of plant cells and human red blood cells respectively. Quantitative phase contrast images of cellular and subcellular organelles of plant cells are observable and quantifiable using MZ-DHIM. From a time series of holograms time varying cell parameters under various conditions can also be studied. Static and dynamic parameters of human red blood cells and can also be extracted using the same microscope. But in the case of MZ-DHIM (where two separate coherent beams are used to generate interference patterns) both the beams travel along different paths and may pick up uncorrelated path length changes even when vibration isolation mechanism is employed. This will lead to reduction in temporal phase stability of the microscope. This in turn may affect its use in measurement of small

cell thickness fluctuations. Also the implementation of two-beam microscope using Mach-Zehnder geometry requires, a number of optical components for beam splitting and beam combining, like mirrors, beam splitters and in some cases two microscope objectives etc., which makes the setup hard to implement and expensive. To overcome the problem of temporal stability, common path interferometric technique can be used [42, 45, 72, 73, 74, 75, 76, 77, 78, 79, 80, 81, 82, 83, 84, 108, 109, 110]. Common path techniques, duplicates the object wavefront and generates the reference wavefront from one of these duplicated wavefronts. It can be done by either by spatially filtering one of the duplicated wavefronts and using it as the reference wavefront [45, 72, 73, 74, 75, 76, 77, 78, 108, 109] or using a portion of the duplicated wavefront (which does not contain object information) as the reference wavefront [42, 77, 79, 80, 81, 82, 83, 84, 110]. Second technique can be termed as self-referencing DHIM. This chapter will first briefly introduce common path self-referencing digital holographic interference microscope using lateral shearing geometry. But this geometry suffers from the reduction of field of view as only half the field of view (in the case of large detector arrays) contains useful object information. Also the reference beam may also contain some information about the medium surrounding the object, which in turn may affect the reconstructed phase profiles. A setup, which is as easy to implement as the self-referencing geometry, but providing the 3D imaging capability of MZ-DHIM will have the potential to provide high quality 3D images with very high temporal stability. Rest of this chapter details the work done on the improvement of field of view of the self-referencing microscope as well as its imaging capability using a pin-hole to filter one of the duplicated beams.

5.2   Lateral Shearing Digital Holographic Microscope

Fig.5.1 presents the basic concept of Lateral shearing digital Holographic microscope [42, 82, 84]. Experimental geometry shown in Fig.5.1 form the basis of the work presented later in this chapter. In the self-referencing geometry, the microscope is very easy to implement. It uses a glass plate to generate two sheared versions of the wavefront that trans-illuminates the object and magnified by the microscope objective

lens. Wavefront reflected by the front and back surfaces of the glass plate are laterally sheared and acquire an angular separation. They travel along the same path and interfere at the detector plane. Part of the object wavefront, unmodulated by object information acts as the reference wavefront. Since the same object wavefront acts as the reference, this setup forms a self-referencing interferometer [42, 82, 84]. Fig.5.1a shows the hologram formed at the digital array (8-bit CCD, 4.65μm pixel pitch) using this microscope. The images from the front and back surfaces of the glass plate can be seen clearly. The object used is glass microspheres (refractive index=1.52) of diameter 10μm immersed in microscope oil (refractive index=1.56). They were imaged using a 40X microscope objective having a numerical aperture of 0.65.
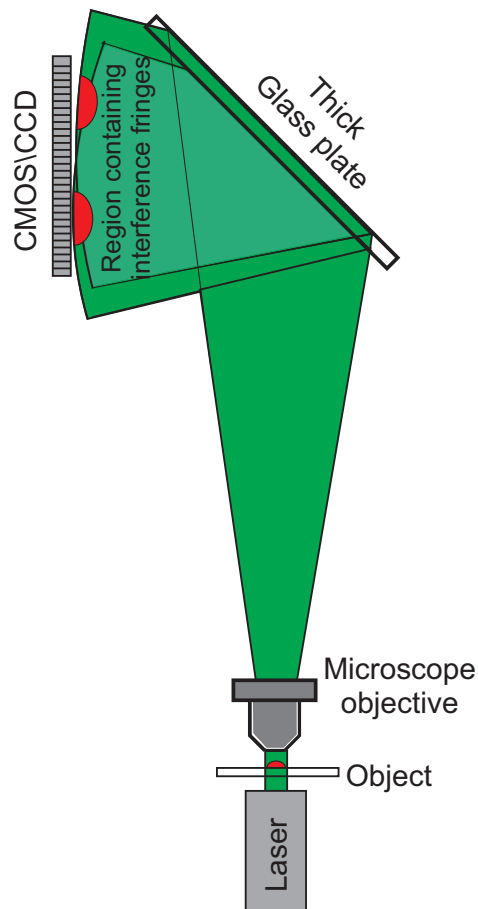

Figure 5.1: Self-referencing Lateral shearing Digital Holographic Microscope [82, 42]

Figs.5.2b and 5.2c show the areas inside the blue rectangles, from which the different curvatures of the fringes can be seen. This is expected as the reference beam (unmodulated portion of the wavefront from the back or front surface) in one case leads the object beam and in the other case lags the object beam.
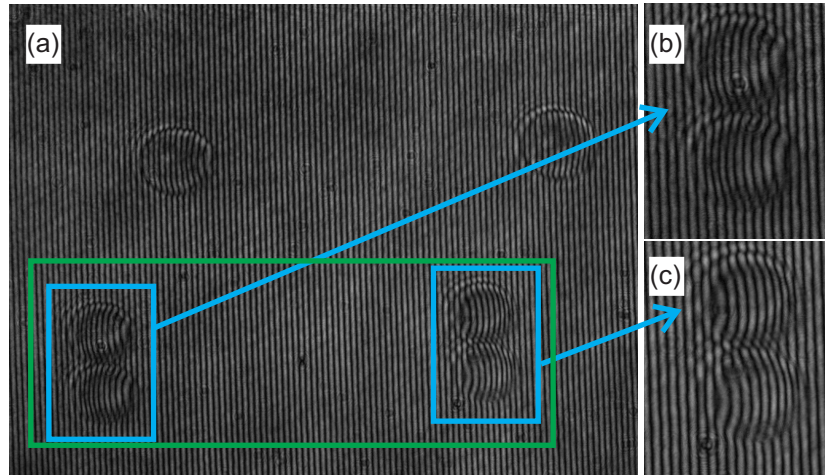

Figure 5.2: Holograms resulting in self-referencing Lateral shearing Digital Holographic Microscope using a glass plate. (a) Recorded hologram (b) and (c) images from the front and back surface of the glass plate (areas inside the blue rectangles).

These holograms are reconstructed as normal digital holograms using ASP integral described in Chapter 2. Fig.5.3a shows continuous phase distribution (obtained by phase unwrapping) after phase subtraction. This when used along with the refractive index values of the microsphere and the surrounding medium (oil), in Eqn.(2.5.3), provides the thickness distribution of the microspheres which is shown in Fig.5.3b. The cross sectional thickness profile of the microsphere along the line in Fig.5.3a is shown in Fig.5.3c. Figs.5.3b and 5.3c shows the three dimensional imaging capability of the technique. The technique works equally well in the case of biological samples also as demonstrated in references [42, 82, 84].

One of the main reasons behind the design of the lateral shearing digital holographic microscope using a glass plate is to exploit its high temporal stability to image the dynamics of cells. So the temporal stability of the technique was measured by recording the holograms of blank microscope slides (recorded at 20Hz for 10s).
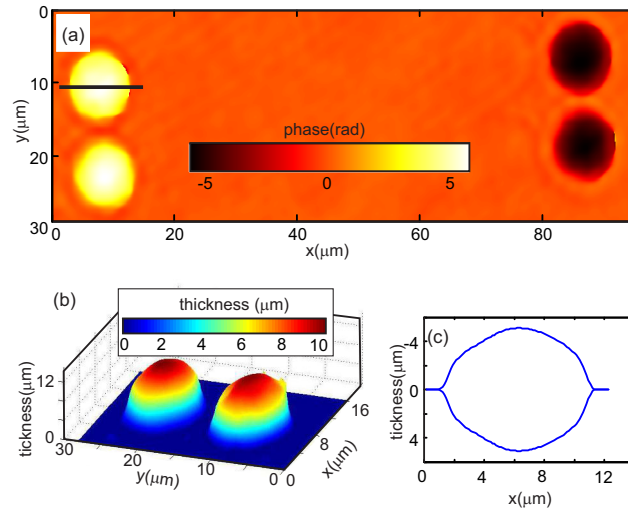
Figure 5.3: Phase contrast images obtained from self-referencing DHIM (a) Phase contrast image (for the area inside the green rectangle) obtained after phase subtraction. (b) Thickness profile of the microspheres. (c) Cross sectional thickness profile of the microsphere.

The mean of the standard deviation of optical path variation for 2500 random points selected from the field of view served as the temporal stability of the system as shown in Fig.5.4.

From Fig.5.1, one can see that, geometry of this set up is simple, easy to implement, containing less number of components and compact. Two beams follow the same direction and encounter same set of optical element to reduce unwanted vibrations in the setup. And results show that the temporal stability is less than 1 nm over period of time 10s, which is suitable to study membrane fluctuations in biological cells. Also the parameters like optical thickness and phase variation shown in Fig.5.3 are comparable with the results of two-beam Mach-Zehnder setup. Thus, for investigating static and dynamic phenomena of low absorbing micro-objects including living cells, it is an ideal tool. But with all these, one has to compromise with the reduced view and overlap of images [42, 82], as hologram is created by two superposed sheared versions of the same object beam. This produces two images of the same object at the hologram plane, making part of the field of view not useful (especially in the case of sensors with large recording area) for object parameter extraction. Also the
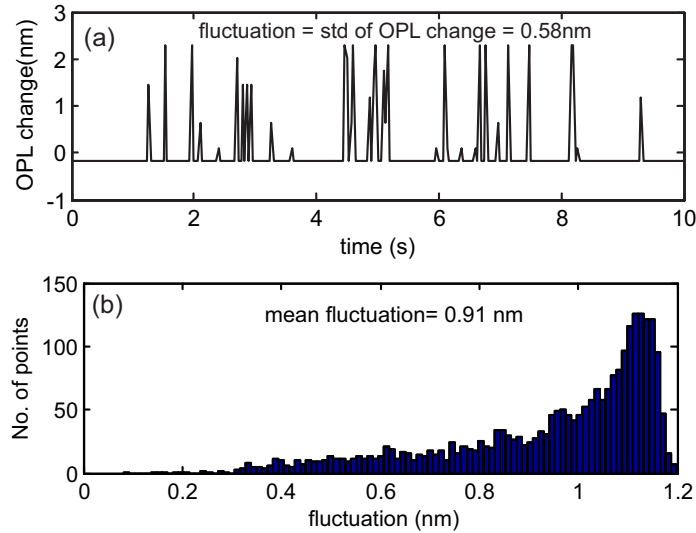
Figure 5.4: (a) Optical path length variation at a single spatial point in the thickness profile; (b) Histogram of the optical path fluctuations at 2500 random spatial points.

reference beam, which is the portion of the object beam not modulated by the object, may contain information about the medium surrounding the object, which may result in unwanted spatial phase variations. To overcome these problems, one of the object beams can be spatially filtered [45, 72, 73, 74, 75, 76, 77, 78, 108, 109] and can be converted to a separate reference beam and made to interfere with object beam at sensor plane. The lateral shearing digital holographic microscope is modified by the use of a pin-hole to create a separate reference beam, while keeping its common path nature intact. It is implemented using a laser diode module as the source. An inexpensive version of the microscope is also made by using of a webcam sensor to record holograms.

5.3 Wide field of view self-referencing digital holographic microscope

Fig.5.5a shows the schematic diagram of wide field of view lateral shearing digital holographic microscope. Photograph of the setup is shown in Fig.5.5b. It uses a laser diode module working at a wavelength of 635nm wavelength (5mW, random linearly

polarized) as the source. A Microscope objective (MO) lens (40X magnification, NA=0.65) is used for object magnification.
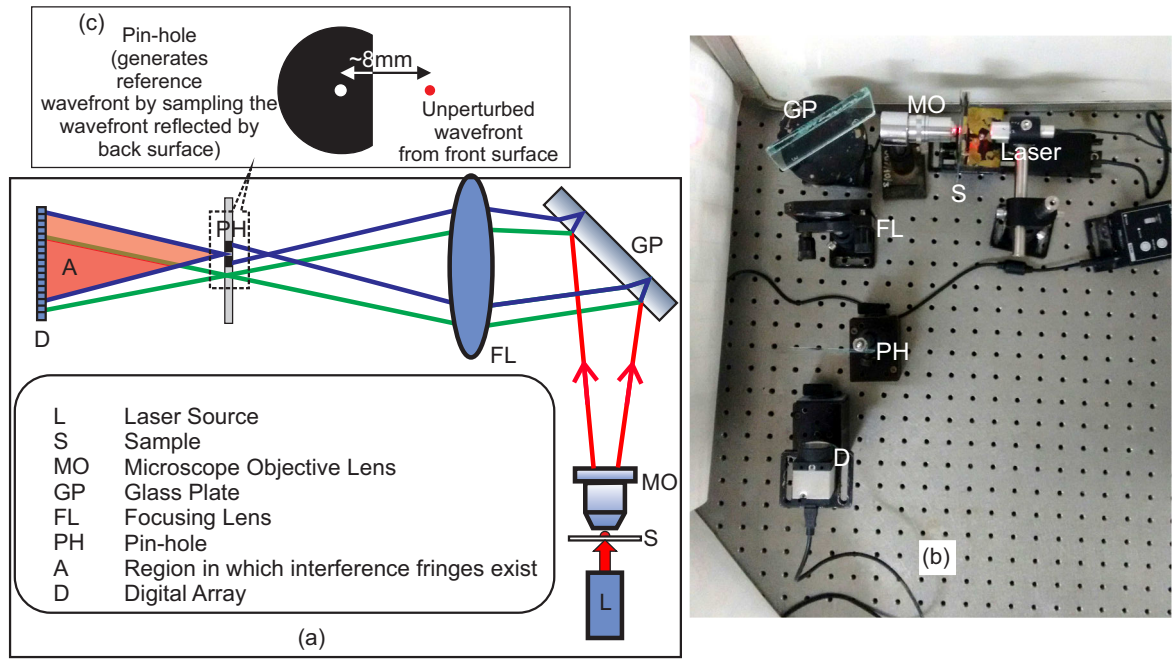

Figure 5.5: Wide field of view Lateral shearing Digital Holographic Interference Microscope. (a) Schematic of the setup. (b) Photograph of the actual setup. (c) Configuration of the pin-hole mounted on a microscope slide used to convert the wavefront reflected from the back surface of the shearing glass plate into the reference wavefront.

The beam from the laser (L) trans-illuminates the object (S) mounted on a translation stage. The sample is magnified by a microscope objective lens (MO). This beam is then is split into two laterally sheared versions by the glass plate (GP) made up of fused silica and thickness of 1cm. Reflections from the front and the back surfaces of the glass plate, travel along the same path, but at a slight angle to each other due to shearing introduced by the glass plate to the spherical wavefront. These two beams are focused by an aspheric lens FL of focal length 12cm having a clear aperture of 5cm. This lens is kept 24cm (MO to front surface of the glass plate to lens) from the objective lens. The beams from the front and back surface of the glass plate travel different distances from the glass plate to reach the focusing lens. The path difference and the lateral separation between the two beams, introduced by the

glass plate, result in the beams coming to focus at different axial as well as lateral positon (Fig.5.5a and Fig.5.5c). Assuming that only a very small portion of wavefront incident on the glass plate is detected by D, the path length difference between the wavefronts, can be deduced using Snell's law and is

$$\delta = n_g 2dcos(\theta_r) \tag{5.3.1}$$

where n_g is the refractive index of the shearing glass plate and d is its thickness. θ_r is the angle of refraction, which depends upon the angle of incidence as well as on the refractive indices of the shearing glass plate as well as the medium surrounding the shearing plate (usually air). For interference fringes to form this path length difference should be less than the coherence length of the laser source.

At the point where the beam from the front surface of the glass plate becomes a point, the lateral separation between it and beam from the back surface of the glass plate is around 8mm. A portion of the wavefront from the back surface is filtered (sampled), using a 30μm diameter pin-hole mounted on a microscope slide (Fig.5.5c), to erase the object information, and is converted into reference wavefront [78]. Beam from the front surface of the glass plate passes through the unobstructed portion of the microscope slide, without any perturbation, carrying all the object information. These two beams superimpose at the detector plane resulting in the formation of holograms. Fig.5.6a and Fig.5.6b shows the intensity of the reference and object wavefront at the detector plane. The hologram formed by their superposition is shown in Fig.5.6c. All the images shown in Fig.5.6 are recorded using an 8-bit CCD array with 4.65μm pixel pitch.

5.4   Calibration of the microscope

System is calibrated by recording the holograms of polystyrene microspheres of diameter 10μm $\pm 0.25\mu$m, immersed in microscope oil. Refractive index of the material of the microsphere is 1.58 and that of the immersion oil is 1.52. Fig.5.7a shows the reconstructed unwrapped phase distribution of the microsphere recorded using a CCD array. This phase distribution is plugged into Eqn.(2.5.2) along with the refractive
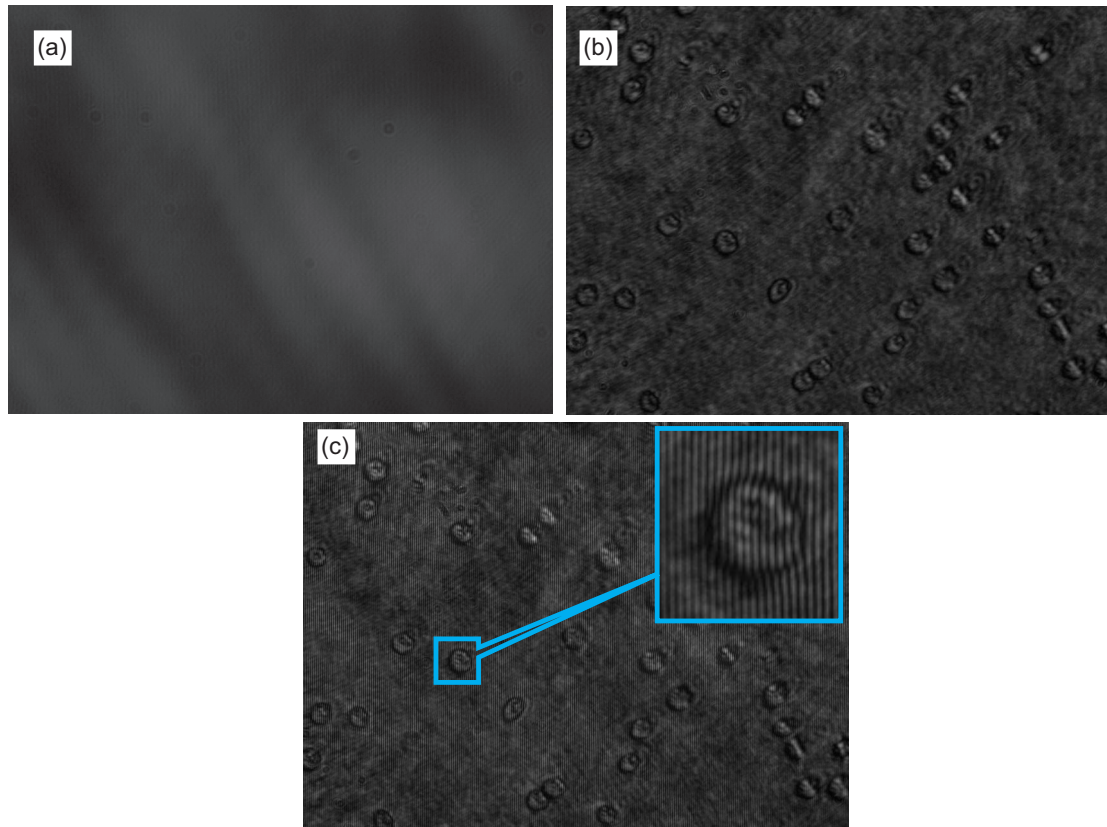
Figure 5.6: Recorded images in the wide field of view lateral shearing digital holographic microscope. (a) Reference beam intensity at the detector plane. (b) Object beam intensity recorded by the detector. (c) Holograms formed at the detector plane.

index values to obtain the thickness profile of the microsphere shown in Fig.5.7b and Fig.5.7c.
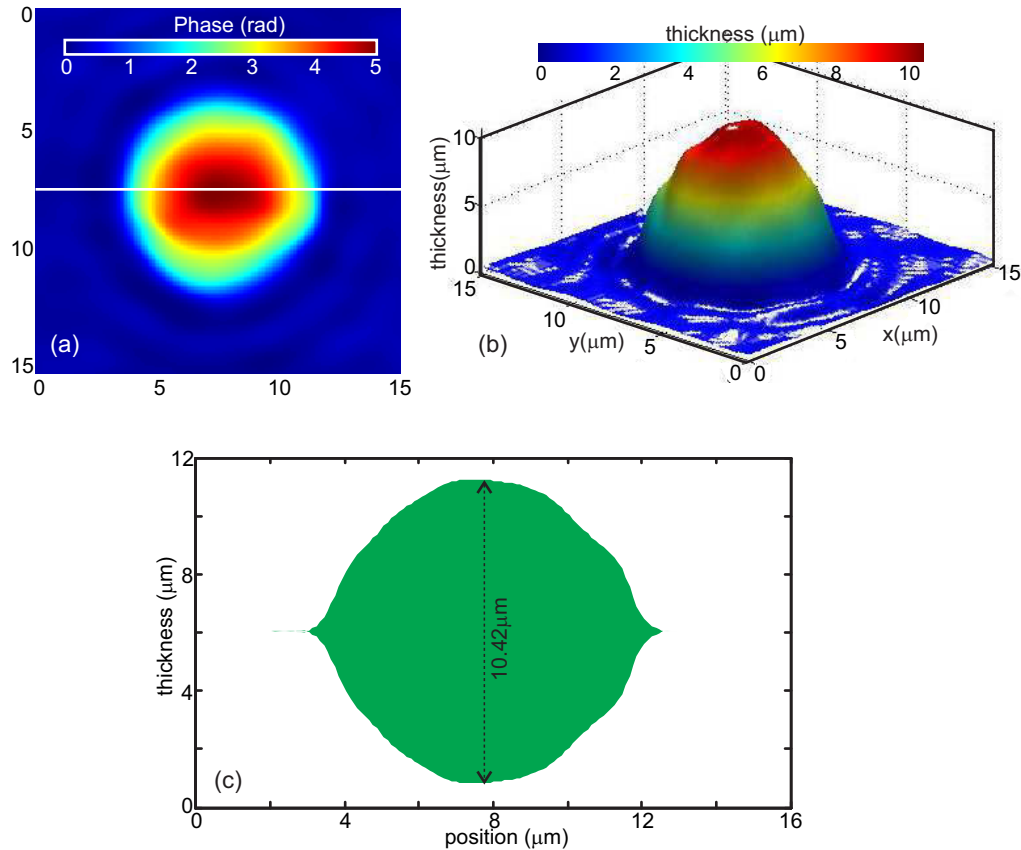

Figure 5.7: Calibration of the wide field of view lateral shearing digital holographic microscope using polystyrene microspheres of 10μm diameter. (a) Quantitative phase profile obtained after phase subtraction. (b) Three dimensional thickness distribution profile of the microsphere obtained from the phase profile. (c) Cross-sectional thickness profile of the microsphere long the line shown in Fig.5.7a.

Thickness measurement was carried out for several microspheres, which provided a mean thickness value of 10.11μm $\pm\ 0.19\mu$m, which is very close to the manufacturer specified value of 10μm, indicating its 3D imaging capability. A low cost version of the microscope is also developed using a VGA webcam sensor (color, pixel pitch 3.2μm) to record holograms. Calibration of the low cost system is also done the same way.

5.5 Spatial and temporal phase stability of the microscope

Spatial phase stability value of the microscope provides its limit on imaging axial thickness variations. It is computed by subtracting the spatial phase variation obtained without microscope slide from the phase variation obtained with a blank microscope slide. Fig.5.8a shows the spatially varying phase distribution obtained with CCD array as the recording device. Histogram of the spatial phase variation is shown in Fig.5.8b and the standard deviation of this phase distribution is its spatial phase stability. The mean of the spatial phase stability computed from several holograms serves as the spatial stability value of the microscope and determines its axial resolution. Spatial stability computations for webcam sensor as the recording device are shown in Fig.5.8c and Fig.5.8d. Table 5.1 gives the values of the spatial stabilities obtained using the two detectors.

Table 5.1: Spatial phase stability of the microscope

Recording devive	Spatial stability	
	Phase (rad)	OPL (nm)
CCD array	0.042±0.0047	4.24±0.47
Webcam sensor	0.053±0.0061	5.36±0.62

Sub-nanometer temporal stabilities are required to study cell membrane fluctuations. One of the advantages of the common path digital holographic microscopes is that they can provide temporal stabilities good enough to image cell membrane oscillations [42, 45, 72, 73, 74, 75, 76, 77, 78, 82, 83, 84, 109, 110]. So measurement of temporal stability of the developed common path system is necessary, before its use in dynamic imaging of cells. For measurement of the temporal phase stability, a time series of holograms with a blank microscope slide (object holograms) in the sample holder is recorded. A hologram recorded without the microscope slide yield the reference phase. As explained in Section 3.5, mean of the standard deviations of the time variation of the phase difference (obtained from hologram recorded at each time instance) computed at several spatial points provides the temporal phase stability. This is repeated by recording several time series and the average of these
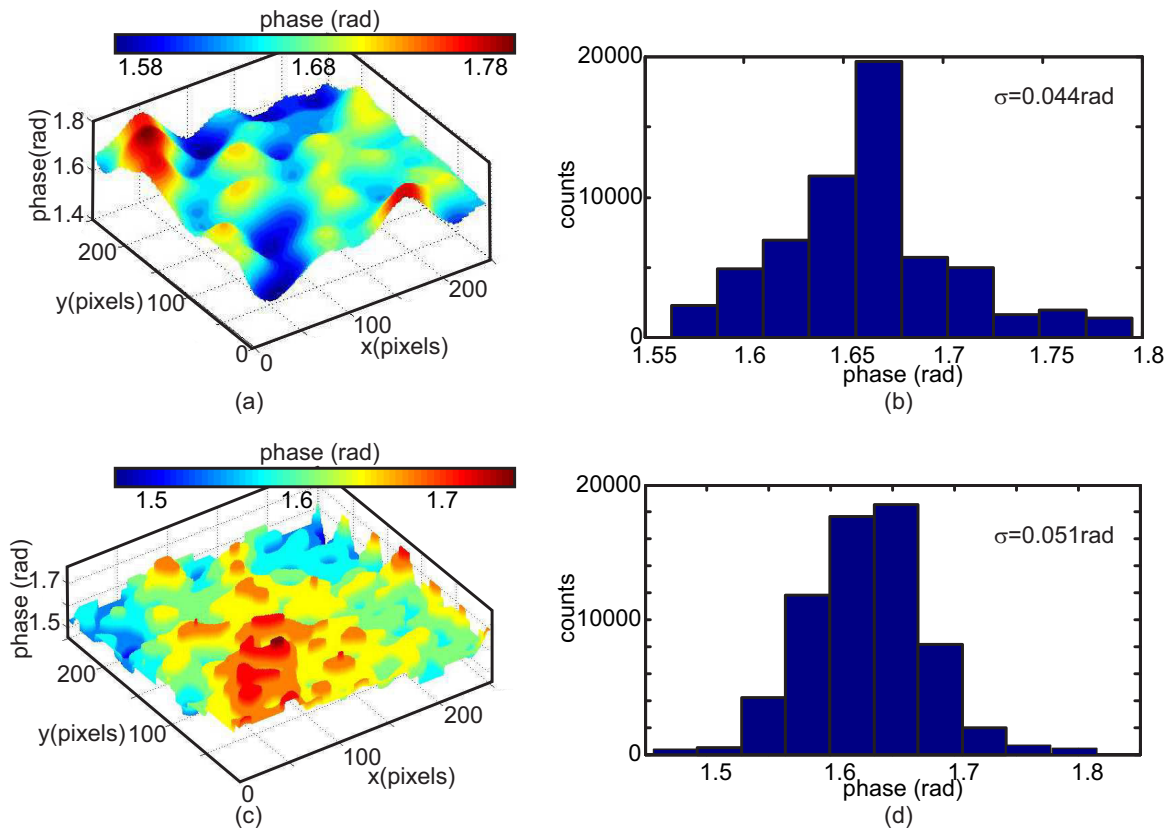
Figure 5.8: Spatial stability of the wide field of view common path digital holographic microscope. Spatial variation of phase computed from holograms recorded using a CCD array and a VGA webcam sensor are shown in (a) and (c) respectively. Histograms of the phase distributions for obtained using CCD array and webcam sensor are shown in (b) and (d) respectively.

phase stabilities is used as the value of the temporal phase stability of the system. For the CCD array, holograms were recorded at the rate of 15Hz for a total period of 30s and in the case of the webcam sensor holograms were recorded at 25Hz for 30s to compute the temporal stability. Fig.5.9 shows the temporal stability measurement of the developed system. Values of the temporal stabilities of the microscopes using different recording mediums system are given in Table 5.2.
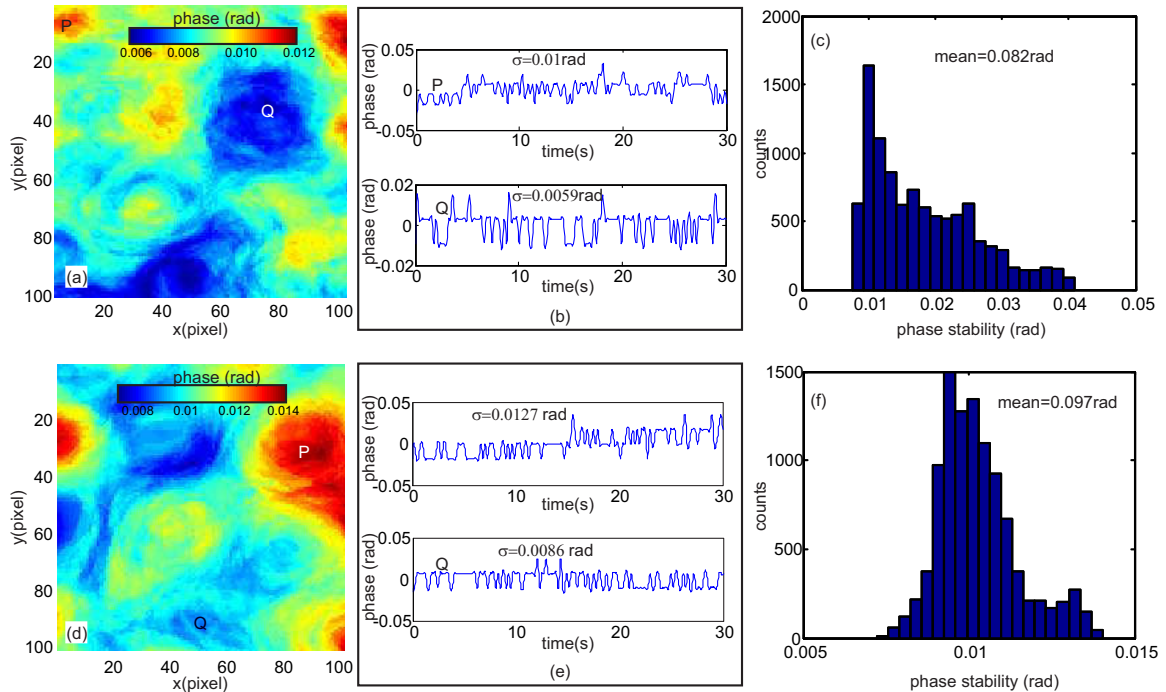

Figure 5.9: Temporal phase stability of the wide field of view common path digital holographic microscope using CCD array (a-c) and VGA webcam sensor (d-f). Spatial variation in the temporal phase stability using a CCD array and a VGA webcam sensor are shown in (a) and (d) respectively. (b) and (e) shows the time evolution of phase. (c) and (f) is the histogram of the temporal phase variation for CCD array and webcam respectively.

Spatial filtering of one of the beams to create a separated reference beam leads to higher spatial stability and the common path nature of the microscope provides sub-nanometer temporal stability.

Table 5.2: Temporal phase stability of the microscope

Recording devive	Temporal stability (30s)	
	Phase (rad)	OPL (nm)
CCD array	0.00821±0.00091	0.829±0.091
Webcam sensor	0.00953± 0.00108	0.963± 0.109

5.6 Imaging of red blood cells using wide field of view microscope

After calibrating the system and determining its spatial and temporal stabilities it is used for 3D imaging of red blood cells and their parameter extraction. The biggest advantage of this microscope is that, its full field of view can be utilized unlike the one employing common lateral shearing geometry [42, 82]. Fig.5.10a shows the hologram of red blood cell distribution (obtained from a healthy individual) recorded using an 8-bit CCD array of pixel pitch 4.65μm. Portion inside the blue rectangle is shown in Fig.5.10b, which clearly shows the interference fringes and their modulation. Quantitative phase contrast image obtained after phase subtraction is shown in Fig.5.10c. Optical thickness distribution computed by plugging this phase distribution into Eqn.(2.5.3) provides the three dimensional profile of the cells (Fig.5.10d).

Low cost version of the microscope is implemented using a VGA webcam (color, 3.2μm pixel pitch) array for recording of the holograms. This configuration has a reduced field of view since the sensor area is smaller compared to that of CCD array. But the cost of the webcam sensor is only a fraction of the CCD array. Fig.5.11a shows the hologram recorded using the webcam array. Region of interest inside the black rectangle is shown in Fig.5.11b, which shows the recorded interference fringes. Obtained quantitative phase profile of the cells after phase subtraction is shown in Fig.5.11c and the optical thickness distribution is shown in Fig.5.11d.

Time variation in the thickness profile, provides the dynamic parameters related to the cells. For the CCD array, holograms were recorded (field of view 1024×768 pixels 150μm×110μm) at the rate of 15Hz for 30s. Reconstructed phase profile is used to compute the spatially varying thickness profile of the cell at each time instance. Fig.5.12a shows the reconstructed phase profile of the cells in the field of view at
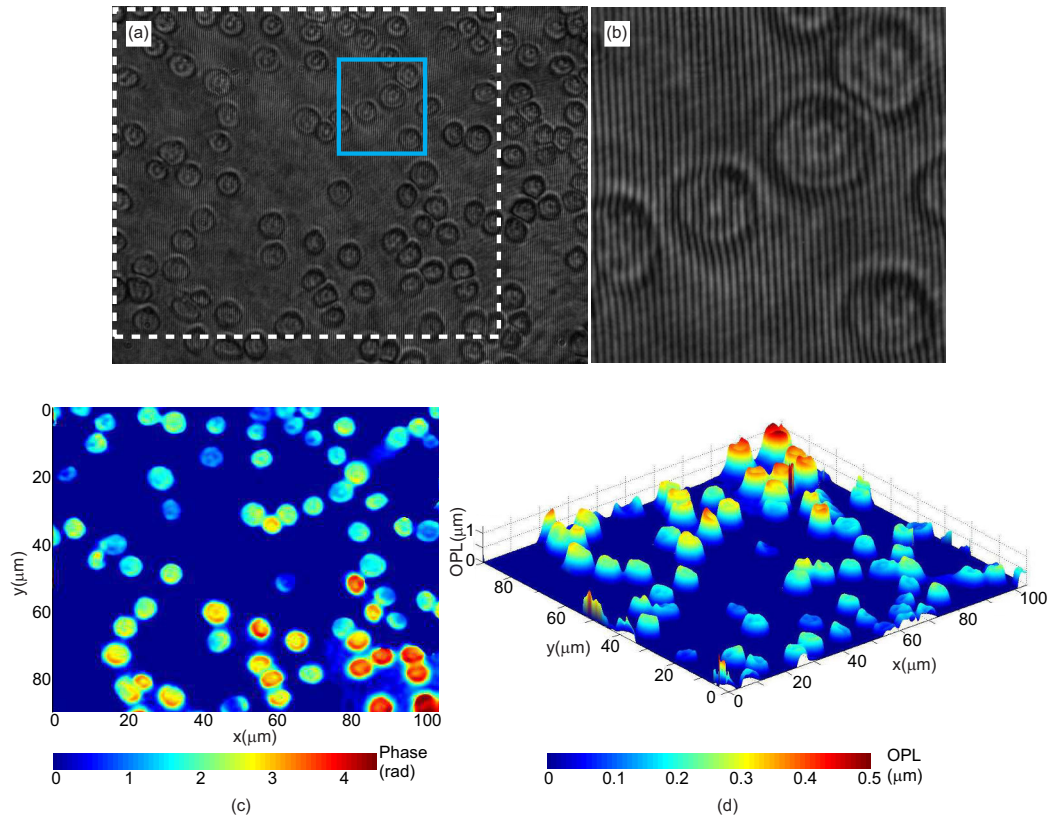
Figure 5.10: (a) Hologram recorded with CCD array. (b) Zoomed region inside the blue rectangle. (c) Quantitative phase distribution inside the white (dashed) rectangle. (d) Optical thickness distribution computed from the quantitative phase information.

one time instance. Each analyzed cell is marked. Inset of the figure shows the three dimensional rendering of the optical thickness distribution of the cell marked inside the rectangle. Fluctuation profile of the cell is obtained by the use of the standard deviation of the time varying thickness profile in Eqn.(4.4.1) and is shown in Fig.5.12b. Inset of this figure shows the three dimensional rendering of the fluctuation profile of the cell inside the rectangle. Optical volume of the cell volume at each time instance is the sum of the thickness at pixel multiplied by area occupied by each pixel, which in turn depends upon the lateral magnification of the system. Fig.5.12c shows the time variation in optical volume of different cells marked in Fig.5.12a. Fourier analysis of the time varying thickness profile provides information about the frequency of
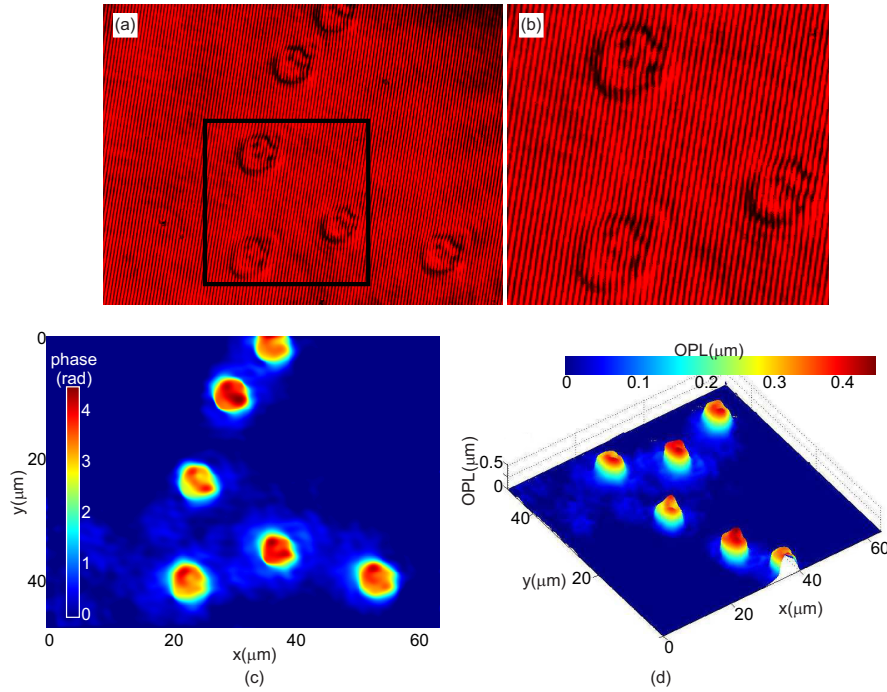
Figure 5.11: Results obtained with Webcam array as the recording device. (a) Hologram recorded with webcam array. (b) Zoomed region inside the black rectangle. (c) Quantitative phase distribution for the hologram shown in Fig. 5.11a. (d) Optical thickness distribution computed from the quantitative phase information.

thickness fluctuations at different points inside the cell as shows in Fig.5.12d. Here also the inset shows the three dimensional rendering of the frequency distribution for the cell inside the rectangle. Measured cell parameters (obtained from 65 cells) are given in Table 5.3.

Healthy red blood distributions are imaged using the microscope employing a VGA webcam array also. The field of view in the case of webcam sensor is approximately $50\mu m \times 65\mu m$. Here also holograms for 30s are recorded but at the rate of 30Hz. Fig.5.13a shows the optical thickness distribution of the healthy red blood cells imaged using the webcam sensor along with the three dimensional visualization of one of the cells (inside the white rectangle). The reconstructed time evolving thickness variation provides the optical thickness fluctuation profile shown in Fig.5.13b, which also shows the three dimensional thickness fluctuation profile for the marked cell.
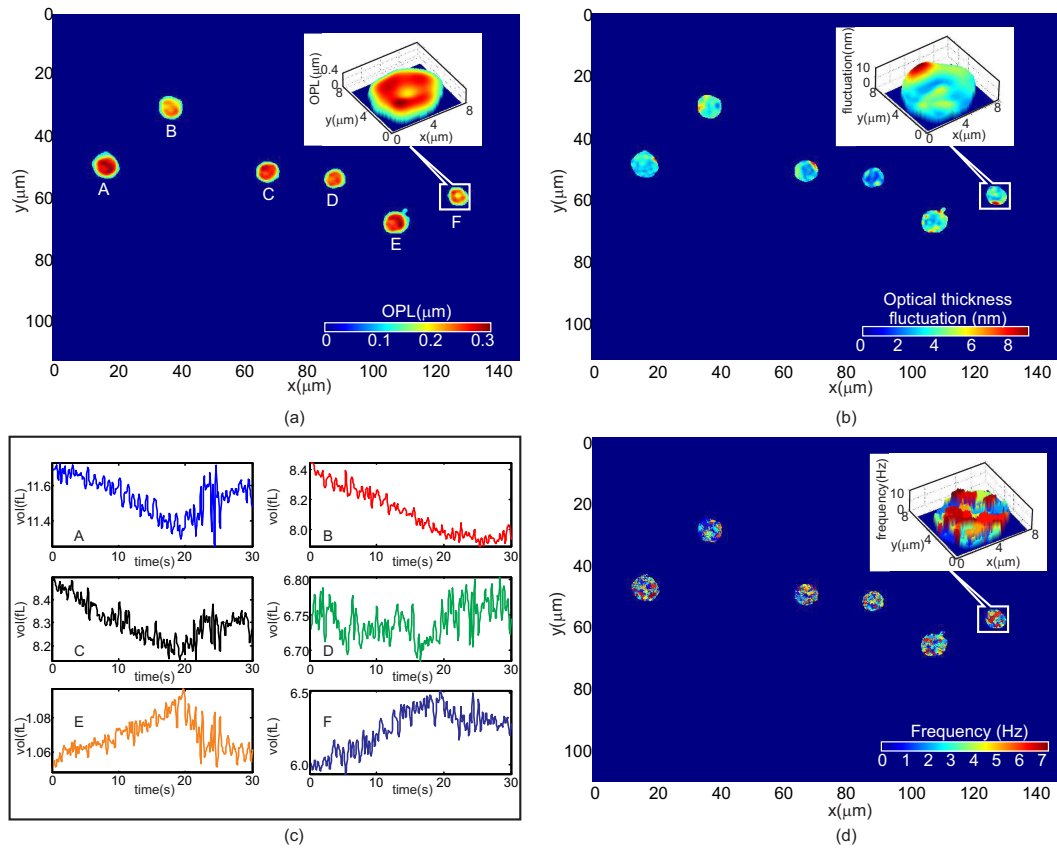
Figure 5.12: Imaging of cell dynamics. (a) Optical path length distribution of the cells in the field of view reconstructed from the phase profile. Inset shows the three dimensional optical thickness profile of the cell inside the region of interest marked by the white rectangle. (b) Optical thickness fluctuation at each point on the cell along with the three dimensional rendering of the optical fluctuation profile for the cell inside the white rectangle. (c) Time variation of optical volume (for the cells marked in Fig. 5.12a). (d) Frequency of thickness oscillations at each point on the cell (inset shows the 3D rendering of the frequency profile for the cell inside the white rectangle.

Time evolving volume for the cells marked (A to E) in Fig.5.13a is shown in Fig.5.13c. Frequency profile of the cells (Fig.5.13d) obtained by Fourier analysis of the time evolving thickness profile at each point on the cell is used to calculate the frequency of optical thickness of the cells. Table 5.3 shows the measured cell parameters for the holograms recorded by the webcam array (for 52 cells).
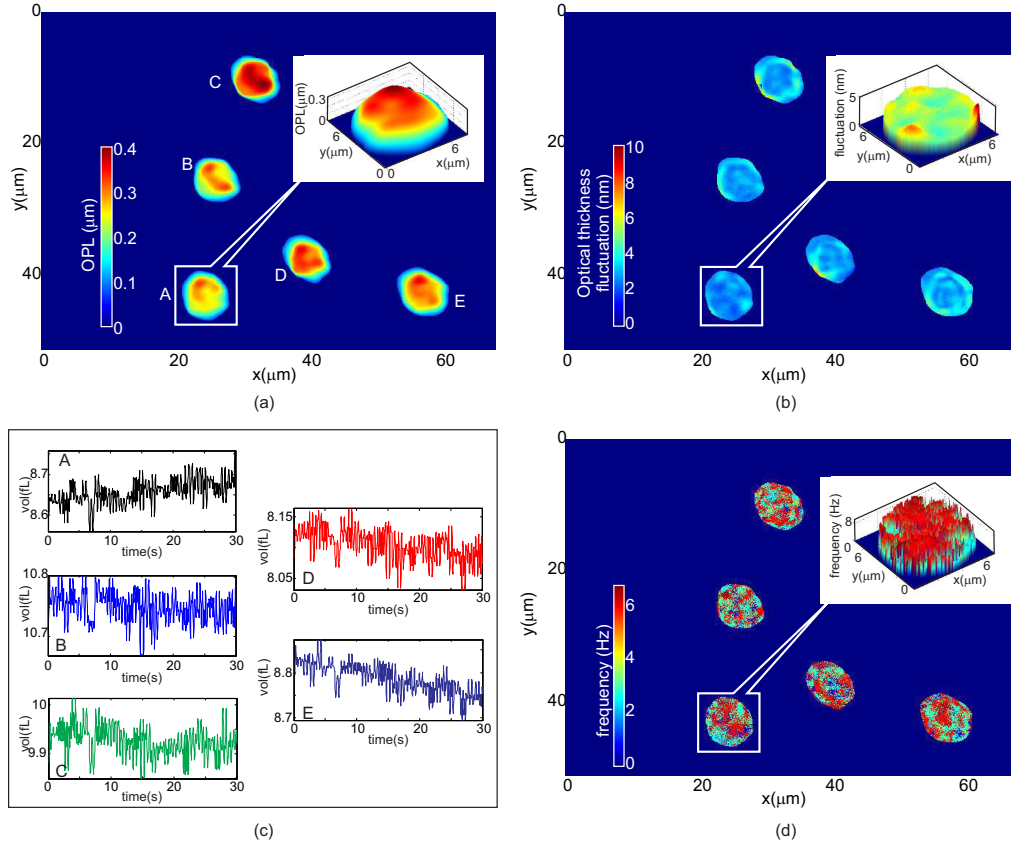

Figure 5.13: Imaging of cell dynamics using webcam array. (a) Optical thickness distribution of the cells in the field of view obtained from the phase profile along with the three dimensional optical thickness profile of the cell inside the region of interest marked by the white rectangle. (b) Optical thickness fluctuation profile of the cells along with the three dimensional rendering of the optical fluctuation profile. (c) Optical volume as a function of time (for the cells marked in Fig.5.13a). (d) Change in frequency of thickness fluctuation with position inside the cells.

Wide field of view lateral shearing digital holographic microscope provides many cell parameters including dynamic parameters as demonstrated in table 5.3. The

Table 5.3: Static and dynamic parameters of healthy red blood cells measured using wide field of view lateral shearing digital holographic microscope

Sr. No.	Parameter	Measured value (mean±std)	
		Using CCD array	Using webcam
1	Diameter (μm)	7.41±0.54	7.56±0.35
2	Mean value of optical thickness (μm)	0.288±0.061	0.259±0.022
3	Coefficient of variation of optical thickness	0.2132±0.032	0.2442±0.028
4	Projected area (μm^2)	43.19±9.41	41.43±5.82
5	Optical volume (fL)	7.64±1.86	8.12±1.06
6	Optical total surface area (μm^2)	88.86±15.67	84.51±9.27
7	Surface area/optical volume ratio $\times 10^6 (m^{-1})$	11.22±0.56	10.85±0.78
8	Sphericity	0.245±0.015	0.258±0.017
9	Amplitude of thickness fluctuation (nm)	3.23±1.03	3.11±1.13
10	Volume fluctuation (fL)	0.106±0.005	0.091±0.006
11	Mean peak frequency of thickness fluctuation (Hz)	3.37±0.91	3.93±0.92

main advantage of this microscope over lateral shearing version is that its whole field of view is useable (no redundant object information), while being temporally stable. Described microscope is more temporally stable in comparison to two-beam Mach-Zehnder based microscope, providing sub-nanometer temporal resolution. This sub-nanometer stability makes it possible to study cell thickness fluctuations accurately, thus optical thickness profile of object along with the time evolution of the thickness profile is obtained. These parameters can provide important information on the state of health of the cells in a sample. Webcam arrays are a cost-effective alternative to CCD arrays to record holograms. Even though the spatial and temporal stability is slightly lower for the device using webcam array, the cell parameters measured were similar to those measured using CCD array, demonstrating its potential for construction of low cost, off-axis (single shot) digital holographic microscopes. The field of view in the case of VGA webcam array less than that of the CCD array, but this can be improved by using megapixel webcam arrays and also by reducing the magnification of the system.